Translational Oncology 46 (2024) 101971

Contents lists available at ScienceDirect

Translational Oncology

journal homepage: www.elsevier.com/locate/tranon

Original Research

Regulation of Hippo–YAP signaling axis by Isoalantolactone suppresses tumor progression in cholangiocarcinoma

Cho-Long Kim [a,1], Su-Bin Lim [a,1], Dong Hyun Kim [a], Ye Eun Sim [a], Li-Jung Kang [b], Su Jung Park [c], Hyungwoo Kim [d], Tae Hoon Roh [e], Jung-Soon Mo [a,f,*], Han-Sol Jeong [c,**]

[a] Department of Biomedical Sciences, Graduate School, Ajou University School of Medicine, Suwon 16499, South Korea
[b] Three-Dimensional Immune System Imaging Core Facility, Ajou University, Suwon 16499, South Korea
[c] Division of Applied Medicine, School of Korean Medicine, Pusan National University, Yangsan 50612, South Korea
[d] Division of Pharmacology, School of Korean Medicine, Pusan National University, Yangsan 50612, South Korea
[e] Department of Neurosurgery, Ajou University School of Medicine, Suwon 16499, South Korea
[f] Institute of Medical Science, Ajou University School of Medicine, Suwon 16499, South Korea

ARTICLE INFO

Keywords:
Cholangiocarcinoma
Isoalantolactone
Hippo-YAP pathway
Apoptosis
Cell growth
Cell migration

ABSTRACT

Cholangiocarcinoma (CCA) is a devastating malignancy characterized by aggressive tumor growth and limited treatment options. Dysregulation of the Hippo signaling pathway and its downstream effector, Yes-associated protein (YAP), has been implicated in CCA development and progression. In this study, we investigated the effects of Isoalantolactone (IALT) on CCA cells to elucidate its effect on YAP activity and its potential clinical significance. Our findings demonstrate that IALT exerts cytotoxic effects, induces apoptosis, and modulates YAP signaling in SNU478 cells. We further confirmed the involvement of the canonical Hippo pathway by generating *LATS1/LATS2* knockout cells, highlighting the dependence of IALT-mediated apoptosis and YAP phosphorylation on the Hippo-LATS signaling axis. In addition, IALT suppressed cell growth and migration, partially dependent on YAP-TEAD activity. These results provide insights into the therapeutic potential of targeting YAP in CCA and provide a rationale for developing of YAP-targeted therapies for this challenging malignancy.

Introduction

Cholangiocarcinoma (CCA) is a highly aggressive and heterogeneous cancer that arises from the biliary epithelium [1,44]. Its late diagnosis, aggressive nature, and resistance to current treatments pose significant challenges in clinical management, resulting in poor prognosis with a median survival of approximately 6 months [6,37]. Therefore, novel therapeutic strategies are urgently needed to improve patient outcomes [45]. Recent research has identified several signaling pathways, including Notch, Hippo, FGF/FGFR, mTOR, and TGF-β pathways, that play critical roles in the development of CCA [27,35,42,46,53]. YAP is upregulated in human colorectal tissue samples, further supporting its role in the proliferation and migration of colorectal cancer cells [14]. Moreover, YAP is associated with poor overall survival and disease-free survival, especially in patients treated with neoadjuvant chemotherapy [29]. Also, various studies have confirmed that prostate cancer relies on YAP hyperactivation, implicating the dysfunction of the Hippo signaling in cancer initiation, progression, metastasis, and resistance to treatment [20]. The dysregulation of these pathways can occur via various mechanisms, presenting new opportunities for targeted therapy [26].

The Hippo pathway, which regulates organ size, cellular proliferation, and apoptosis through its effector protein, YAP, has emerged as a critical factor in the development of CCA [30,39]. YAP functions as a transcriptional co-activator and promotes the expression of genes related to cell growth, survival, and metastasis [9]. Aberrant YAP activity has been linked to tumor initiation, progression, and poor prognosis in CCA, with overexpression and activation of YAP frequently observed in CCA cells, particularly in the nuclear compartment (nuclear

Abbreviations: CCA, cholangiocarcinoma; IALT, isoalantolactone; LATS1/LATS2, large tumor suppressor kinase 1/2; MAP4Ks, mitogen-activated protein kinase kinase kinase kinases; MOB1A/B, Mps one binder kinase activator-like 1A/B; MST1/MST2, mammalian sterile twenty-like kinase 1/2; YAP, Yes-associated protein.

* Corresponding author at: Institute of Medical Science, Ajou University School of Medicine, Suwon 16499, South Korea.
** Corresponding author.
E-mail addresses: j5mo@ajou.ac.kr (J.-S. Mo), jhsol33@pusan.ac.kr (H.-S. Jeong).
[1] These authors contributed equally to this work.

https://doi.org/10.1016/j.tranon.2024.101971
Received 18 January 2024; Received in revised form 12 April 2024; Accepted 17 April 2024

YAP) [35,36,39]. Multiple studies have identified increased activity of YAP in CCA, making it a potential therapeutic target due to its association with tumor initiation, progression, and poor prognosis [8,38,40,43]. These findings highlight the significance of targeting YAP as a potential therapeutic strategy for CCA.

Natural products have been used as medicines for various diseases and cancer treatments for thousands of years, particularly in Asia, including countries like Korea, China, and Japan. Research on these natural products has been conducted alongside various chemotherapies, exploring diverse mechanisms of action [11]. Isoalantolactone (IALT) is a natural compound derived from medicinal plants, particularly in the *I. helenium* and *Inula racemose Hook. f.* [15], shows promising anticancer properties in various cancer types [3]. Its diverse pharmacological properties include anti-inflammatory [10], antioxidant [51], antimicrobial [23], and anticancer activities [33]. Numerous studies have reported its inhibitory effects on cell proliferation, apoptosis induction, and modulation of various signaling pathways in different cancer cell lines [5,16,21,22,47,49,50,52]. Furthermore, the combination of IALT with cisplatin has proven more effective in overcoming cisplatin-resistant in ovarian cancer, significantly reducing tumor growth in resistant xenograft models [7]. These findings highlight the potential of IALT as a multi-target therapeutic agent for cancer treatment.

Given the promising anticancer effects of IALT and the dysregulation of the Hippo-YAP pathway in CCA, this study aimed to investigate the effects of IALT on Hippo-YAP signaling in SNU478 cells, a well-established CCA cell line. We demonstrated that IALT exhibited cytotoxic effects in SNU478 cells by inducing cell death through caspase-dependent apoptosis. Furthermore, IALT promotes the phosphorylation of YAP and inhibits its nuclear translocation suppressing of cell growth and proliferation. Overall, our study provides novel insights into the molecular mechanisms underlying the anticancer effects of IALT and suggests that targeting Hippo-YAP signaling with IALT could be a promising therapeutic strategy for treating of CCA and potentially other cancers exhibiting dysregulated Hippo-YAP signaling.

Material and methods

Antibodies

LATS1 (#3477), LATS2 (#5888), phospho-LATS1 (Thr1079, #8654), MST2 (#3952), MAP4K4 (#5146), PARP (#9532), MOB1 (#13730), phospho-MOB1 (Thr35, #8699), YAP (#14074), phospho-YAP (Ser127, #4911), and YAP/TAZ (#8418S) were purchased from Cell Signaling Technology (Berverly, MA, USA). CYR61 (sc-13100), HA probe (sc-57592), and YAP1 (sc-101199) were obtained from Santa Cruz Biotechnology, Inc. (Santa Cruz, CA, USA). Vinculin (V9131) was purchased from Sigma-Aldrich (St. Louis, MA, USA). Caspase-3 (31A1067) was purchased from Novus Biologicals (Littleton, CO, USA). MST1 (#3681) and TEF-1 (#610922) were obtained from BD Biosciences (San Jose, CA, USA). Horseradish peroxidase-conjugated secondary antibodies (NA931V and NA934V) were purchased from GE Healthcare (Chicago, IL, USA). Alexa Fluor 488-conjugated goat anti-mouse IgG (H + L) antibody (A11029) and Alexa Fluor 594-conjugated goat anti-rabbit IgG (H + L) antibody (A11037) were purchased from Invitrogen (Carlsbad, CA, USA).

Chemicals

Isoalantolactone (IALT) was purchased from MedChemExpress (HY-N0780; MCE, Monmouth Junction, NJ, USA) and Sigma-Aldrich (470–17–7; Burlington, MA, USA). Phos-tag-conjugated acrylamide was purchased from Wako Chemicals (304–93521; Richmond, VA, USA).

Cell culture and transfection

SNU478, SNU478 *LATS1/LATS2* KO, SNU1079, and SNU1196 were cultured in RPMI media 1640 containing 10 % fetal bovine serum (FBS), 50 units/mL penicillin, and 50 μg/ml streptomycin (Gibco, Billings, MT, MA, USA). HEK293A *MAP4K4/6/7* KO, HEK293A *MST1/MST2* KO, HEK293A *LATS1/LATS2* KO, HEK293A, and HEK293T were cultured in Dulbecco's modified Eagle's medium containing 10 % FBS, 50 units/mL penicillin, and 50 μg/ml streptomycin (Gibco, Billings, MT, USA). The cells were humidified in 5 % CO_2. HEK293A, HEK293A *MAP4K4/6/7* KO, HEK293A *MST1/MST2* KO, HEK293A *LATS1/LATS2* KO, and HEK293T were provided by Dr. Kun-Liang Guan's laboratory at the University of California San Diego [31], and SNU478, SNU1079, and SNU1196 cells were obtained from the Korean Cell Line Bank (KCLB; Seoul, South Korea). Plasmid transfection was performed with a suitable concentration of each plasmid DNA using a polyethylenimine reagent (PEI, Polysciences, Inc., Warrington, PA, USA) according to the manufacturer's instructions.

CRISPR/Cas9 system

SNU478 *LATS1/LATS2* KO cells were generated using the CRISPR/Cas9 system. We designed an sgRNA using the CRISPR design tool and cloned it into the pSpCas9 (BB)-2A-Puro (PX459; plasmid #62988) and lentiCRISPR V2 vectors (plasmid #52961) supplied by Addgene (Watertown, MA, USA). The cloned lentivirus, generated from the lentiCRISPR V2 vector, was transfected into SNU478 cells. After 24 h of transfection or infection, SNU478 cells were selected for 2 d in media containing puromycin (InvivoGen, San Diego, CA, USA). The cells were then sorted into single cells.

Retroviral infection and generation of stable cell lines

To form retroviruses, HEK293T cells were transfected with the pPGS-HA vector or HA-TEAD1ΔC-YAP (AD) constructs, a viral envelope, and viral packaging using polyethylenimine (PEI, Polysciences, Inc., Warrington, PA, USA). After 48 h incubation, the retroviral supernatant was filtered through a 0.45-μm syringe filter and used to infect HA-TEAD1ΔC-YAP (AD) SNU478 cells with polybrene (Sigma-Aldrich, Burlington, MA, USA). Infected cells were selected using G418 (Gold Biotechnology, Inc., St Louis, MI, USA) in culture medium. This method was used in this study [18].

Cell lysis and western blotting

Cells were lysed in lysis buffer (40 % glycerol, 8 % SDS, 20 % β-mercaptoethanol, 0.2 M Tris (pH 6.8), 0.04 % bromophenol blue). Cell lysates were heated at 100 °C and centrifuged at 13,000 rpm for 5 min. Cell lysates were resolved using SDS-PAGE on 8–15 % gels and transferred to PVDF membranes. After blocking with 5 % skim milk in 1X TBS-T on the shaking machine, the blots were incubated with primary antibodies at 4 °C overnight on the shaking machine. The next day, the blots were washed thrice and incubated with anti-rabbit or anti-mouse HRP-conjugated secondary antibodies diluted 1:5000 in 5 % skim milk in 1X TBS-T at room temperature. The blots were detected using Immobilon Western Chemiluminescent HRP Substrate (Millipore, Burlington, MA, USA). Phos-tag gels were prepared according to the manufacturer's instructions. Band intensities were quantified using the ImageJ software.

MTT assay

SNU478 WT and SNU478 *LATS1/LATS2* KO cells were seeded into 96-well plates. Next day, the plate was treated with diverse concentration of IALT and incubated at 37 °C. After 2 d, yellow tetrazolium salt (3-(4,5-dimethylthiazol-2-yl)−2,5-diphenyltetrazolium bromide; MTT) (T-

030–5, Gold Biotechnology, Inc., St Louis, MI, USA) was added to the plate. The absorbance was measured at 570 nm using a microplate spectrophotometry (BioTek Instruments, Winooski, VT, USA). The IC50 values were calculated from the concentration response curves using Prism 8.4.3 software.

Cell apoptosis assay

The experiment was performed according to the protocol of the FITC Annexin V Apoptosis Detection Kit (#556547; BD Biosciences). SNU478 WT and *LATS1/LATS2* KO cells were seeded in 6-well plates and treated with 0 (DMSO), 5, and 10 μM of IALT for 48 h. Cells attached to the plate were digested with trypsin and centrifuged to collect the cells. The pellet was washed with PBS, repeated, and resuspended in 1X binding buffer. Next, 3 μL each of PI and Annexin V were added per sample, and early and late apoptosis of cells was observed using a BD FACSAria™ III Cell Sorter (BD Biosciences, San Jose, CA, USA) at the Three-Dimensional Immune System Imaging Core Facility of Ajou University (Suwon, South Korea).

Immunoprecipitation (IP)

To assess the interaction between proteins, the cells were lysed in a mild lysis buffer (10 mM Tris at pH 7.5, 1 mM Na_3VO_4, 100 mM NaCl, 1 mM EDTA, 50 mM NaF, 1 % NP-40, and 2 μg/ml Leupeptin, Aprotinin) and centrifuged for 15 min at 4 °C and 13,000 rpm. The supernatants were immunoprecipitated with antibodies for 2 h at 4 °C in a 360° shaking machine. Protein A/G magnetic beads (Thermo Fisher Scientific, Inc., Waltham, MA, USA) were washed using mild lysis buffer and the beads were added in a proper amount for 1 h at 4 °C in a 360° shaking machine. The immunoprecipitates were washed thrice with mild lysis buffer, and the samples were eluted with protein sample buffer.

Immunocytochemistry

SNU478 WT and *LATS1/LATS2* KO cells were seeded on coverslips in a six-well culture plate. The cells were fixed with 2 % formaldehyde for 15 min at room temperature and permeabilized with 0.2 % Triton X-100 for 5 min. After blocking with 10 % FBS in 1X PBS for 30 min, the cells were incubated with the primary antibodies in blocking buffer overnight at 4 °C. The cells were then washed with 10 % FBS in 1X PBS and incubated with Alexa Fluor 488-conjugated goat anti-mouse IgG (H + L) and Alexa Fluor 594-conjugated goat anti-rabbit IgG (H + L) secondary antibodies for 1 h 30 min at 25 °C. The cells were washed with 1X PBS thrice and counterstained with 4',6-diamidino-2-phenylindole (DAPI, Tocris, Bristol, UK) for 2 min to stain the nuclear DNA. The coverslips were mounted by Gel/Mount (Biomeda, San Jose, CA, USA) and then dried on 4 °C. Microscopy was performed using an LSM980 NLO multiphoton microscope (Carl Zeiss, Oberkochen, Germany) at the Three-Dimensional Immune System Imaging Core Facility of Ajou University (Suwon, South Korea). The ZEN (blue edition) program was used for data analysis.

RNA isolation and qRT-PCR

Total RNA was extracted using the TRIzol reagent (Invitrogen, MA, USA). cDNA was synthesized from 1 μg of total RNA using reverse transcriptase, 25 mM $MgCl_2$, 5X Reaction buffer (Promega, Madison, WI, USA), recombinant RNase inhibitors, dNTPs, and random primers (Takara Bio, Shiga, Japan). qRT-PCR was performed using the KAPA SYBR FAST qPCR Master Mix (2X) kits (KAPA Biosystems, Rhoche, Basel, Switzerland) with a suitable pair according to the manufacturer's instructions, and the data were collected using the StepOnePlus real-time PCR system. *Hypoxanthine-guanine phosphorylated ribosyltransferase 1* expression was used for normalization. The sequences of the qPCR primers are as follows:

Primer	Forward (5′→3′)	Reverse (5′→3′)	Refs.
CTGF	CCAATGACAACGCCTCCTG	TGGTGCAGCCAGAAAGCTC	[28]
CYR61	AGCCTCGCATCCTATACAACC	TTCTTTCACAAGGCGGCACTC	[28]
HPRT	AGAATGTCTTGATTGTGGAAGA	ACCTTGACCATCTTTGGATTA	[28]

Sulforhodamine B assay

SNU478 WT and SNU478 *LATS1/LATS2* KO cells were seeded in 96-well culture plates. The plates were incubated at 37 °C and harvested every 2 d at the same time. Next, the plates were fixed with 10 % trichloroacetic acid solution (Sigma-Aldrich, Burlington, MA, USA) at 4 °C overnight and washed with distilled water thrice. The cells were stained with 0.4 % sulforhodamine B (SRB, Sigma-Aldrich, Burlington, MA, USA) in 0.1 % acetic acid solution for approximately 30 min in the dark at room temperature and then dissolved in 10 mM Trizma base (Sigma-Aldrich, Burlington, MA, USA) on a shaking machine for at least 1 h. Absorbance of the resolved cells was measured at 540 nm using a microplate spectrophotometry (BioTek Instruments, Winooski, VT, USA).

Wound healing assay

SNU478 cells expressing the pPGS-HA (empty vector) or HA-TEAD1ΔC-YAP (AD) were cultured on 12-well plates and incubated at 37 °C to reach approximately 90 % confluence. The cells were scratched using an autoclaved tip, and the medium in the plates was changed to remove the cells that fell off. The scratched sections were observed for 48 h using a ZEISS Celldiscover7 microscope (Carl Zeiss, Oberkochen, Germany) at the Three-Dimensional Immune System Imaging Core Facility of Ajou University (Suwon, South Korea) and the growing cells were analyzed via the ZEN 3.5 (blue edition) program.

Clonogenic cell survival assay

SNU478 WT and SNU478 *LATS1/LATS2* KO cells were seeded in a 12-well plate and incubated at 37 °C for approximately 2 weeks. During incubation, the medium with IALT was changed every 3 d. After approximately 2 weeks, the cells were stained with 0.25 % crystal violet (Junsei, Tokyo, Japan) for 5–10 min and then washed with distilled water until background removal. The cells were destained with 95 % ethanol for 1 h on a shaking machine, and the absorbance of the destaining solution was measured using a microplate spectrophotometry (BioTek Instruments, Winooski, VT, USA) at 595 nm.

TA cloning

The AccuRapid TA cloning kit (K-7170; Bioneer, Daejeon, South Korea) was used. First, genomic DNA was extracted from knockout cells using AccuPrep® Genomic DNA Extraction Kit (20020E, Bioneer, Daejeon, South Korea), and PCR was performed using Taq polymerase (PCRBIO, London, UK). Next, the PCR products were isolated using the Prep GEL/PCR Purification Mini kit (FAGCK001–1, FAVORGEN, Vienna, Austria) to obtain insert DNA, which was confirmed using electrophoresis. After mixing the pBHA-T vector and the reaction buffer containing T4 ligase with the insert DNA, the mixture was incubated overnight at 16 °C. Then, the recombinant plasmid was transformed into competent DH5α bacteria and spread on ampicillin-containing LB agar plates with 50 μL of IPTG (0.1 M, Gold Biotechnology, Inc., St Louis, MI, USA) and X-Gal (50 mg/μL, LPS Solution, Daejeon, South Korea) to distinguish colonies and incubated at 37 °C. After overnight incubation, white colonies with inserts were collected from the plate, and colony PCR was performed. White colonies subjected to PCR were identified via gel electrophoresis, compared to positive controls, and analyzed using

the National Center for Biotechnology Information basic local alignment search tool.

Tumor isolation from mouse

BALB/c nude mice (5-week-old, 18–21 g) were purchased from Orient Bio, Inc. (Shizuoka, Japan). Six-week-old male nude mice were subcutaneously injected with 2 x 10^6 cells of SNU478 cultured *in vitro*. After 24 d of cell injection, mice were randomly divided into two groups ($n = 5$/group). IALT (10 mg/kg) diluted in less than 5 % DMSO (Sigma-Aldrich, Burlington, MA, USA) and sunflower seed oil were administered intraperitoneally once every 3 d to each group (IALT). Mice in the control group (Con) were injected with less than 5 % DMSO and sunflower seed oil only. The size of the tumor was measured every 4 d. Mice were euthanised 24 d after drug administration, and the weight of the tumor was analyzed. The animal experimental protocol used in this study has been reviewed by the Laboratory Animal Research Center of Ajou University Medical Center on their ethical procedures and scientific care, and it has been approved (Protocol Number 2022–0087).

Statistical analysis

Statistical analysis was performed using GraphPad Prism software, version 8.4.3 (GraphPad Software, San Diego, CA, USA). The results are presented as mean ± standard error of the mean (SEM) of three separate experiments or three independent biological replicates. Statistical analysis was carried out using Student's *t*-test (unpaired, two-tailed) or two-way analysis of variance, with $^*P < 0.05$, $^{**}P < 0.01$, $^{***}P < 0.001$, and $^{****}P < 0.0001$ indicating statistical significance. No statistical method was used to determine the sample size. The investigators were blinded to the allocation during the experiments and outcome assessments.

Results

Effects of IALT on SNU478 cell viability and apoptosis induction

We evaluated the cytotoxicity of IALT, a sesquiterpene lactone derived from medicinal plants, such as *Inula helenium* and *Vernonia amygdalina,* in SNU478 cells (Fig. 1A). Cell viability was assessed by subjecting the cells to different concentrations of IALT using the MTT assay. After 48 h of incubation, the IC50 value of IALT was determined to be 58.2 μM (Fig. 1B). Furthermore, the apoptotic potential of IALT was evaluated by Annexin V/PI staining and by examining the expression levels of apoptosis-related proteins, specifically PARP and cleaved caspase-3 (Figs. 1C and 1D). In the absence of IALT, SNU478 cells remained viable, whereas annexin V-positive apoptosis was induced in the presence of IALT (Fig. 1C). Additionally, we conducted western blot analysis to assess caspase activation during apoptosis and observed the presence of cleaved caspase-3 in IALT-treated cells. Caspase activation was further validated by the cleavage of PARP, a caspase-3 substrate (Fig. 1D). Remarkably, IALT demonstrated considerable capacity to induce apoptosis, as evidenced by the pronounced cleavage of PARP and caspase-3 at a concentration of 10 μM (Fig. 1D). These findings provide robust evidence of the apoptotic effects of IALT in SNU478 cells.

IALT induces YAP phosphorylation and inhibits YAP-TEAD transcriptional complex in CCA cells

We explored the inhibitory effects of IALT on YAP, a protein known to be activated in CCA cells, such as SNU478 cells. The phosphorylation status of YAP was assessed using a Phos-tag gel shift assay and immunoblotting with a pYAP (S127) antibody. Our results demonstrated concentration-dependent phosphorylation of YAP and TAZ in response to IALT treatment in SNU478 cells (Figs. 2A and S1A). Similar effects

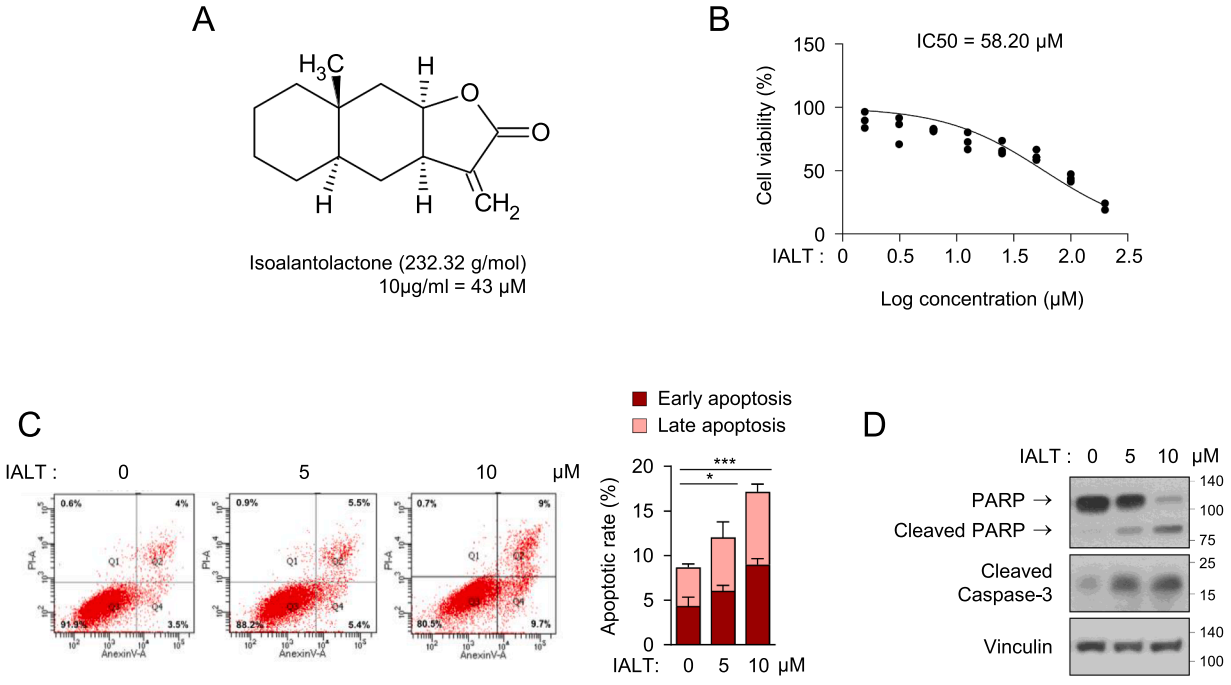

Fig. 1. Isoalantolactone (IALT) promotes cell apoptosis in SNU478 cells. (A) Chemical structure of IALT. (B) The effect of IALT on cell proliferation was measured using MTT assay. SNU478 cells were treated with different concentrations of IALT for 48 h. IC50 values were calculated in nonlinear regression analysis for dose-response inhibition from the OD values using Prism 8.4.3 software. The IC50 values in SNU478 cells were 58.2 μM. Data represent the means ± SEM. ($n = 3$ – n is the number of technical replicates). Each have 3 biological replicates. (C, D) IALT induced cell death. Cell apoptosis distributions were determined via flow cytometry using Annexin V/PI staining. The graph showed increased rate of early and late apoptotic cells after 0 (DMSO), 5, and 10 μM of IALT treatment for 48 h. Data represent the means ± SEM of triplicate experiments (C). Data represent the means ± SEM. ($n = 3$ – n is the number of biological replicates). $^{***}P < 0.001$. $^*P < 0.05$. Student's *t*-test (unpaired, one-tailed) was used for statistical analysis. SNU478 cells were treated with 0, 5, and 10 μM of IALT for 72 h. Cell lysates were immunoblotted (D). Vinculin was used as the loading control. ($n = 3$ – n is the number of biological replicates).

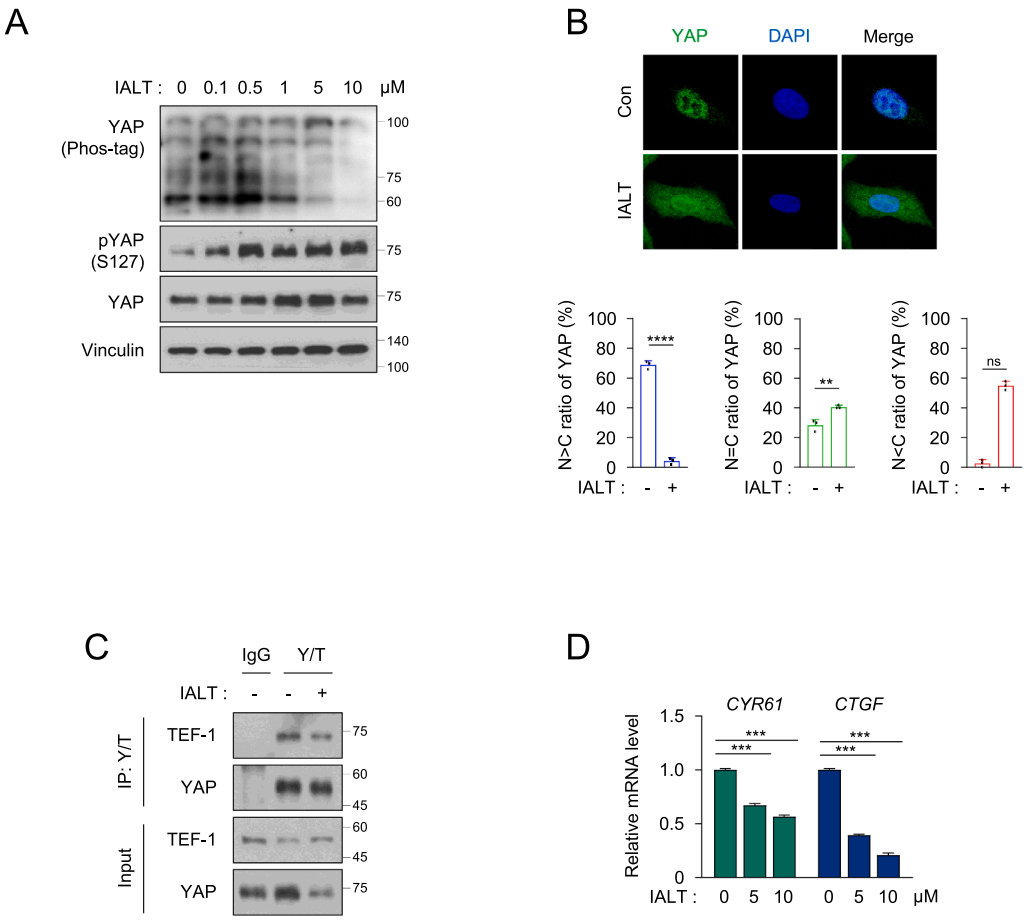

Fig. 2. IALT phosphorylates YAP and prevents YAP–TEAD interaction. (A) SNU478 cells were treated with 0, 0.1, 0.5, 1, 5, and 10 μM of IALT for 12 h. Cell lysates were immunoblotted and YAP phosphorylation states were determined by Phos-tag gel. ($n = 3$ – n is the number of biological replicates). (B) SNU478 cells were treated with 2 μM IALT for 3 h and stained with YAP (green) and DAPI (blue). YAP localization was detected via immunocytochemistry using LSM980 NLO. The nuclear (N)-cytoplasmic (C) ratio of YAP was analyzed in three randomly selected fields of one experiment (100 cells per field). Scale bars, 10 μm. $^{****}P < 0.0001$. $^{**}P < 0.01$. ns: Not significant. Student's *t*-test (unpaired, one-tailed) was used for statistical analysis. (C) SNU478 cells were treated with IALT (10 μM) for 12 h and was immunoprecipitated using anti-YAP/TAZ Abs. ($n = 3$ – n is the number of biological replicates). (D) The mRNA levels of CYR61 and CTGF were determined via qRT-PCR in SNU478 cells treated with 0, 5, and 10 μM of IALT for 12 h. Error bars are shown as mean ± SEM. ($n = 3$ – n is the number of technical replicates). Each have 2 biological replicates. $^{***}P < 0.001$. Student's *t*-test (unpaired, one-tailed) was used for statistical analysis.

were observed in both SNU1079 and SNU1196 cells, another CCA cell line, further supporting the ability of IALT to induce YAP phosphorylation (Figs. S1B-S1E). These findings confirm that IALT induces YAP phosphorylation in CCA cells. To investigate the effects of IALT treatment on the subcellular localization of phosphorylated YAP, we conducted immunofluorescence staining experiments. In the absence of IALT, YAP is predominantly localized to the nucleus. However, IALT treatment resulted in a significant translocation of YAP from the nucleus to the cytoplasm (Fig. 2B). These results suggest that IALT treatment induced cytoplasmic sequestration of YAP, potentially influencing its transcriptional co-activator function. Importantly, the subcellular localization of YAP is closely associated with its transcriptional activity as it translocates to the nucleus and forms a complex with the transcription factor TEAD, thereby facilitating gene transcription [17]. Consistent with this, IALT treatment reduced the interaction between YAP and TEAD (Fig. 2C). Additionally, IALT treatment downregulated the mRNA levels of *CYR61* and *CTGF*, two YAP-dependent genes (Fig. 2D). Collectively, these results indicated that IALT inhibited the YAP-TEAD transcriptional complex, thereby influencing downstream gene expression. In summary, these findings suggest that IALT induces YAP phosphorylation, disrupts its interaction with TEAD, and modulates the expression of downstream target genes in SNU478 cells.

IALT activates the canonical Hippo pathway to inhibit YAP activity and downstream gene expression

We investigated the inhibitory effects of IALT on YAP phosphorylation using knockout (KO) HEK293A cell lines targeting key components of the Hippo signaling pathway, including MST1/MST2, MAP4K4/6/7, and LATS1/LATS2 [31]. The effect of IALT on YAP phosphorylation was assessed using Phos-tag gel shift assays and immunoblotting with specific antibodies such as pYAP (S127), pMOB (T35), and pLATS1 (T1079). Our results revealed that IALT-induced YAP phosphorylation was less effective in *MST1/MST2* KO and *LATS1/LATS2* KO cells compared to that wild-type cells (Fig. S2A). Notably, IALT induced YAP phosphorylation in *MAP4K4/6/7* KO cell lines, suggesting that MST1/MST2 primarily mediates LATS1 phosphorylation after IALT treatment. To assess the functional implications of IALT-mediated YAP phosphorylation in HEK293A *MST1/MST2* KO and HEK293A *LATS1/LATS2* KO cell lines, we examined the mRNA levels of *CYR61* and *CTGF* using RT-qPCR. Inhibition of *CYR61* and *CTGF* expression by IALT was significantly reduced in both HEK293A *MST1/MST2* KO and HEK293A *LATS1/LATS2* KO cell lines compared to that in HEK293A wild-type cells (Fig. S2B), further supporting the involvement of MST1/MST2 and LATS1/LATS2 in the inhibitory effects of IALT on YAP-dependent gene expression. Subsequently, we utilized SNU478 cell lines with *LATS1/LATS2* knockout using CRISPR/Cas9 technology to

assess the impact of IALT on YAP phosphorylation mediated by LATS1/LATS2 (Fig. S3A). In these SNU478 *LATS1/LATS2* KO cells, IALT failed to induce YAP phosphorylation (Fig. 3A). Additionally, the ability of IALT to retain YAP in the cytoplasm was lost in *LATS1/LATS2* KO cells, resulting in the predominant nuclear localization of YAP (Fig. 3B).

We further evaluated the response of SNU478 *LATS1/LATS2* KO cells to varying concentrations of IALT and found that the IC50 value of IALT was 100.7 μM (Fig. 3C). Moreover, the cytotoxic effect of IALT was reduced in SUN478 *LATS1/LATS2* KO cells compared to that in wild-type cells, as observed in the MTT assay and morphological assessment (Figs. 1B, 3C, and S3B). In addition, the apoptotic effects of IALT were attenuated in *LATS1/LATS2* knockout cells, as demonstrated by PI and Annexin V double staining, as well as by reduced levels of cleaved PARP and cleaved caspase-3, compared to the wild-type cell line (Figs. 3D and 3E). Overall, our results suggest that IALT inhibited YAP activity by activating the canonical Hippo pathway, leading to YAP phosphorylation and the subsequent modulation of downstream gene expression. These findings provide valuable insights into the molecular mechanisms underlying the inhibitory effects of IALT on YAP function.

IALT suppressed cell growth, migration, and tumor growth by inhibiting YAP activity in CCA cells

To evaluate the biological effects of IALT on cell growth, we conducted a clonogenic growth assay using SNU478 WT and SNU478 *LATS1/LATS2* KO cells. Interestingly, the inhibitory effect of IALT on cell growth was attenuated in the SNU478 *LATS1/LATS2* KO cells, as illustrated in Fig. 4A. Furthermore, we investigated the effects of IALT through a proliferation assay. The results showed that the deletion of *LATS1/LATS2* in SNU478 cells was not affected by IALT, whereas SNU478 WT cells exhibited a decrease in proliferation upon IALT compared with the control SNU478 WT cells (Fig. S4A). To explore the role of YAP-TEAD activity in the inhibition of cell migration by IALT, we introduced active YAP-TEAD fusion protein (TEAD1ΔC-YAP (AD)) into SNU478 cells (Fig. S4B). Remarkably, the migration-inhibitory effect of IALT was abolished in SNU478 cells expressing TEAD1ΔC-YAP (AD), indicating that the suppression of migration of IALT was mediated through the inhibition of YAP-TEAD activity (Fig. 4B). Furthermore, in an immunocompromised nude mouse xenograft model, injection of SNU478 cells led to tumor development (Fig. 4C). Consistent with our *in vitro* findings, the administration of IALT significantly reduced the growth of xenografted tumors in these mice, providing further evidence for the ability of IALT to inhibit YAP activity *in vivo* (Figs. 4D-G). Collectively, these results highlight the ability of IALT to impede tumor progression by modulating YAP activity.

Discussion

The transcriptional co-activator YAP has emerged as a critical regulator of various cellular processes, including cell proliferation, differentiation, and organ size control [9,17,25]. In numerous malignancies including CCA, the enhanced activity of the YAP has been implicated in tumor initiation, metastasis, and resistance to conventional therapies [25,39]. Elevated nuclear YAP levels are correlated with histological differentiation, TNM stage, metastasis, and poor prognosis in CCA. In the specific context of SNU478 cells, a CCA cell line, previous studies have shown the overexpression and activation of YAP, suggesting that the dysregulation of YAP contributes to the aggressive phenotype of this cancer.

IALT elicited apoptosis in SGC-7901 gastric cancer cells and Hep3B hepatocellular carcinoma cells through mitochondrial pathways, the PI3K/Akt pathway, or via activation of the ROS-dependent JNK pathway, respectively [19,34]. Additionally, in prostate cancer cells, it exerts apoptotic effects via ROS-mediated ER-stress [5]. Dysregulation of the Hippo-YAP pathway is commonly observed in gastric cancer [24], while YAP1's significant involvement in liver cancer stem cells is underscored by its overexpression, which correlates with poor prognosis and drug resistance [48]. Similarly, abnormalities in Hippo pathway signaling in prostate cancer are associated with disease progression and drug resistance, with perturbed YAP/TAZ activity promoting epithelial-mesenchymal transition (EMT), invasion, and metastasis, contributing to unfavorable clinical outcomes [20]. These findings highlight the multifaceted anticancer properties of IALT and its potential as a promising therapeutic agent for various malignancies.

Our study aimed to investigate the effects of IALT on the Hippo-YAP signaling pathway and its implications in cell growth, migration, and tumor progression in CCA cell lines. Our findings demonstrated that IALT exerts inhibitory effects on YAP through the canonical Hippo-LATS signaling pathway, leading to the modulation of downstream gene expression and cellular responses. IALT induced YAP and TAZ phosphorylation in a concentration-dependent manner in both HEK293A and SNU478 cells (Figs. 2A, S1A, and S2A). However, this effect was significantly reduced in cells lacking the key components of the Hippo pathway, namely MST1/MST2 and LATS1/LATS2 (Fig. S2A). This suggests that the canonical Hippo signaling cascade plays a pivotal role in IALT-mediated YAP phosphorylation and that MST1/MST2 and LATS1/LATS2 are critical regulators of this process. Further investigations into the detailed molecular mechanisms underlying the activation of the Hippo-LATS pathway by IALT and its effects on YAP phosphorylation are warranted to gain a deeper insight into the mode of action of IALT.

In addition to inducing YAP phosphorylation, IALT treatment led to the cytoplasmic sequestration of phosphorylated YAP, impairing its nuclear translocation and transcriptional co-activator functions (Fig. 3A). This observation indicated that IALT effectively disrupted YAP-TEAD transcriptional activity by targeting the Hippo-LATS pathway. Consistent with the inhibitory effects on YAP activity, IALT treatment resulted in significant downregulation of YAP-dependent gene expression, including *CYR61* and *CTGF*, in both HEK293A and SNU478 cells (Figs. 2D and S2B). Importantly, these effects were attenuated in *MST1/MST2* and *LATS1/LATS2* KO cell lines, further supporting the involvement of these key components in the regulation of YAP activity by IALT. Furthermore, IALT-induced YAP phosphorylation inhibited cell growth, migration, and tumor progression (Fig. 4). In clonogenic growth assays, IALT significantly suppressed the growth of wild-type SNU478 cells, but its effect was weaker in *LATS1/LATS2* KO cells, suggesting that the inhibition of cell growth by IALT partly relies on LATS1/LATS2-dependent YAP phosphorylation (Fig. 4A). Additionally, the inhibitory effect of IALT on migration was abolished in cells expressing the active YAP-TEAD fusion protein, providing direct evidence of the fact that the suppression of migration of IALT is linked to its inhibition of YAP-TEAD activity (Fig. 4B).

In an immunocompromised mouse xenograft model, IALT administration significantly reduced the growth of xenograft tumors, further supporting the potential of IALT as a therapeutic agent against tumor progression (Fig. 4C). The *in vivo* results were consistent with the *in vitro* findings, highlighting the significant anti-tumor effects of IALT through the inhibition of YAP activity. Expanding *in vivo* studies to different tumor models, such as patient-derived xenografts or genetically engineered mouse models, could provide a more comprehensive understanding of the therapeutic potential of IALT in diverse cancer types and genetic backgrounds. Combination therapy, exploring IALT in combination with other targeted therapies or conventional chemotherapeutic agents, may offer synergistic effects for cancer treatment. Investigating the molecular interactions and signaling pathways involved in combination therapies could lead to more effective and personalized treatment strategies.

The development of YAP inhibitors holds significant promise for cancer treatment, given the pivotal role of the Hippo-YAP signaling pathway in tumorigenesis and cancer progression. Several approaches are under exploration, including small molecule inhibitors, peptides, and monoclonal antibodies. Notably, small-molecule inhibitors disrupting the YAP-TEAD interaction have shown efficacy in preclinical

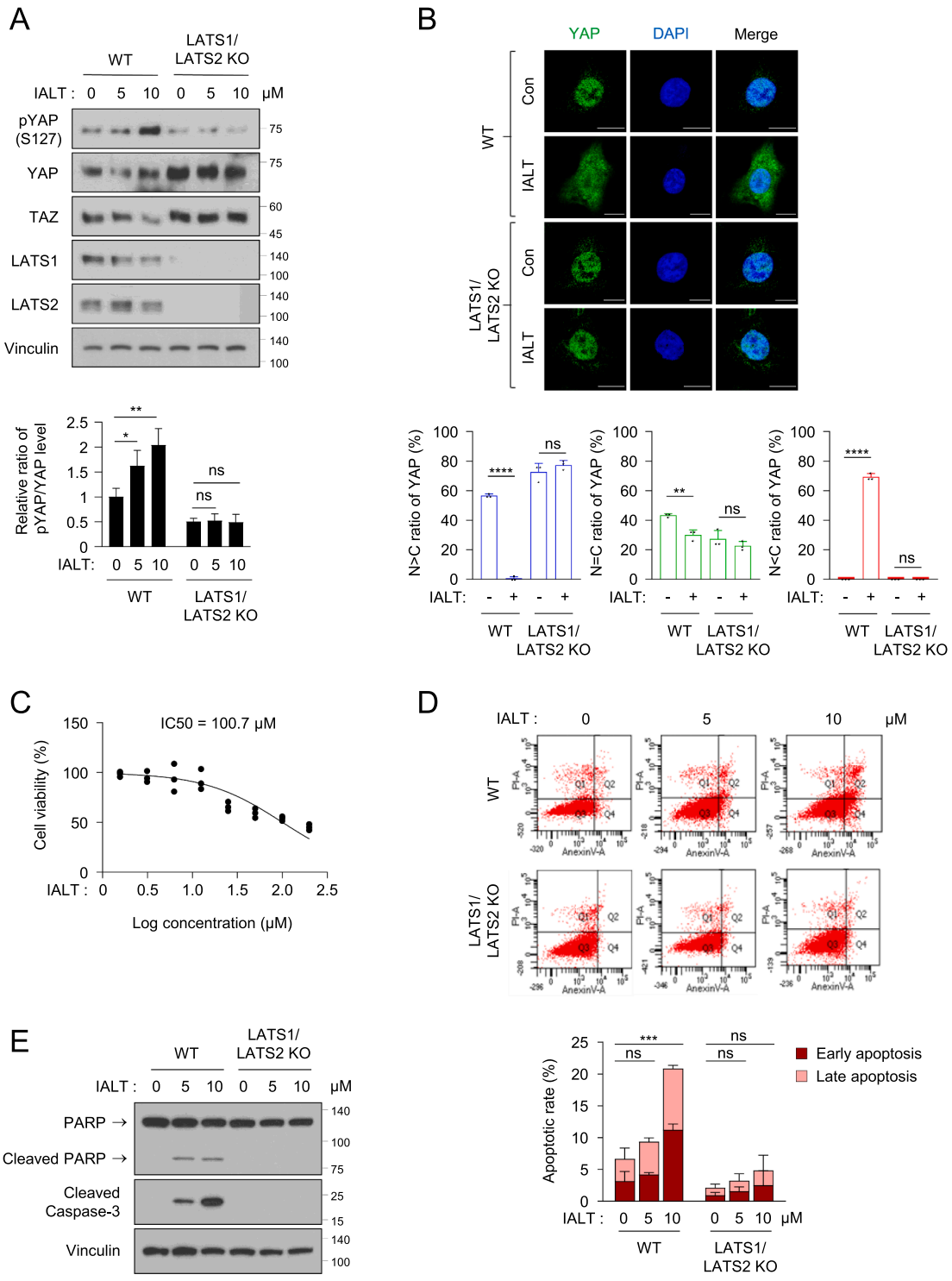

Fig. 3. MST1/MST2 and LATS1/LATS2 regulate the impact of IALT on YAP phosphorylation in SNU478 cells. (A) SNU478 WT and *LATS1/LATS2* KO cells were treated with 0, 5, and 10 μM of IALT in serum starvation media for 12 h, and whole cell lysates were immunoblotted. ($n = 3$ – n is the number of biological replicates). $^{**}P < 0.01$. $^{*}P < 0.05$. ns: Not significant. Student's *t*-test (unpaired, one-tailed) was used for statistical analysis. (B) SNU478 WT and *LATS1/LATS2* KO cells were treated with 2 μM for 3 h and stained with YAP (green) and DAPI (blue). YAP localization was detected via immunocytochemistry using LSM980 NLO. The nuclear (N)-cytoplasmic (C) ratio of YAP was analyzed in three randomly selected fields of one experiment (100 cells per field). Scale bars, 10 μm. $^{****}P < 0.0001$. $^{**}P < 0.01$. ns: Not significant. Student's *t*-test (unpaired, one-tailed) was used for statistical analysis. (C) The effect of IALT on cell viability was measured using an MTT assay. SNU478 *LATS1/LATS2* KO cells were treated with diverse concentrations of IALT for 48 h. IC50 values were calculated in nonlinear regression analysis for dose-response inhibition from OD value using Prism 8.4.3 software. The IC50 value of SNU478 *LATS1/LATS2* KO cells was 100.7 μM ($n = 3$ – n is the number of technical replicates). Each has 3 biological replicates. (D-E) Cell apoptosis by IALT enhances in wild-type (WT), not *LATS1/LATS2* KO. Cell apoptosis distributions were determined via flow cytometry using Annexin V/PI staining. SNU478 WT and *LATS1/LATS2* KO cells were treated with 0, 5, and 10 μM of IALT for 48 h (D). Error bars are shown as mean ± SEM. ($n = 3$ – n is the number of biological replicates). $^{***}P < 0.001$. ns: Not significant. Student's *t*-test (unpaired, one-tailed) was used for statistical analysis. WT and *LATS1/LATS2* KO of SNU478 cells were treated with 0, 5, and 10 μM of IALT for 72 h. Cell lysates were immunoblotted to analyze cell apoptosis, and cleaved PARP and caspase-3 were increased only in WT (E). ($n = 2$ – n is the number of biological replicates).

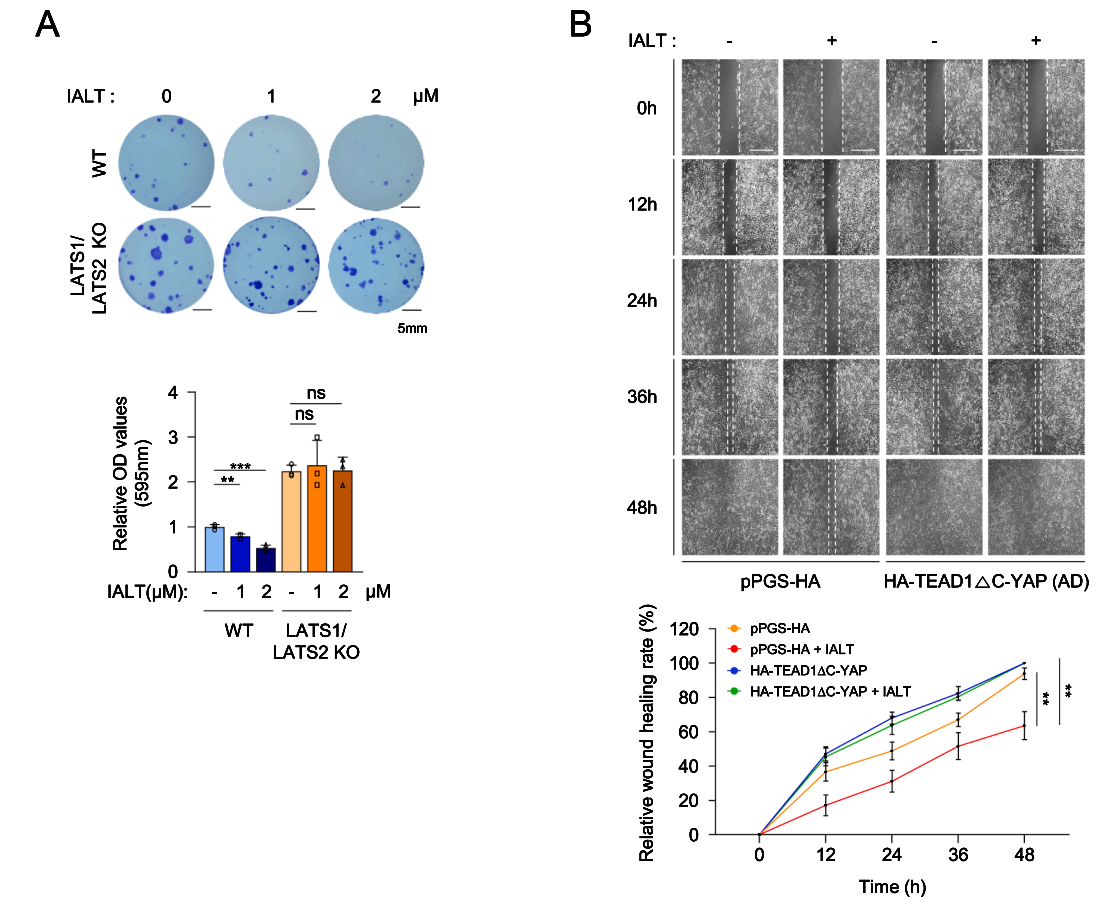

(caption on next page)

Fig. 4. IALT inhibits tumor progression by regulating YAP activity *in vitro* and *in vivo*. (A) The colony formation capacity of SNU478 WT cells was reduced by 1 μM or 2 μM of IALT, but not *LATS1/LATS2* KO. The SNU478 WT and *LATS1/LATS2* KO cells were incubated for almost 2 weeks and stained with 0.25 % crystal violet for 10 min. Subsequently, the cells were destained with 95 % ethanol and destaining solution was measured using a microplate spectrophotometry (BioTek Instruments) at 595 nm of absorbance. Error bars depict mean ± SEM. ($n = 3$ – n is the number of biological replicates). ***$P < 0.001$. **$P < 0.01$. ns: Not Significant. Student's *t*-test (unpaired, one-tailed) was used for statistical analysis. Scale bars, 5 mm. (B) Cell migration of SNU478 cells expressing the pPGS-HA (empty vector) or HA-TEAD1ΔC-YAP (AD) was analyzed via wound healing assay. The cells were wounded and treated with 10 μM of IALT for 48 h. Photographs of scratched section were taken at different time points (0, 12, 24, 36, and 48 h) using ZEISS Celldiscover7 microscope (Carl Zeiss, Three-Dimensional Immune System Imaging Core Facility). Relative wound healing rate was analyzed using ZEN 3.5 (blue edition) program. Error bars depict mean ± SEM. ($n = 3$ – n is the number of biological replicates). **$P < 0.01$. Student's *t*-test (unpaired, one-tailed) was used for statistical analysis. Scale bars, 10 μm. (C-F) IALT inhibits tumor growth *in vivo*. The image was dissected tumors from BALB/c nude mice 48 d after injection of SNU478 cells (C). Mean tumor weights were lower when treated with IALT than those in controls (D). Error bars depict mean ± SEM ($n = 5$). *$P < 0.05$. Student's *t*-test was used for statistical analysis. No significant differences were identified between the two groups of mouse body weights for 48 d (E). When drug treatment was performed 24 d after cell injection; the tumor size of the IALT-treated group was significantly smaller than that of the control group (F). Error bars depict mean ± SEM ($n = 5$ – n is the number of biological replicates in mice tumor). ***$P < 0.001$. Student's *t*-test was used for statistical analysis (F). Phosphorylation of YAP increased with drug-induced tumor size reduction. Tumor tissues isolated from mice were lysed, and the expression levels of pYAP, YAP, and CYR61 were detected via immunoblotting (G). ($n = 2$ – n is the number of biological replicates).

models, offering potential therapeutic avenues [32]. Researchers identified a small molecule pan-TEAD inhibitor that disrupts the interaction between YAP/TAZ and TEAD proteins. This study demonstrates the potential of targeting TEADs as a therapeutic approach for cancer treatment [13]. Verteporfin, an inhibitor of YAP-TEAD and TAZ-TEAD interaction, presents another promising option by impeding invasive tumor perineural invasion (ITPN) [12]. Recent research focuses on developing small molecules hindering the palmitoylation of the TEAD to interfere with the YAP-TEAD interaction [2,4]. However, pharmacological blockade of TEAD-YAP reveals its therapeutic limitations, as seen in the activation of the PI3K/AKT signaling cascade, fostering cancer cell survival and drug resistance [41]. Consequently, efforts to develop combination therapies or multi-target inhibitors are imperative to overcome these limitations, with ongoing investigations into therapies targeting the YAP/TAZ-TEAD signaling axis. Additionally, IALT exhibits potential in modulating upstream regulators of YAP, such as LATS kinases, inducing YAP phosphorylation and inactivation. Furthermore, IALT's induction of apoptosis in cancer cells may contribute to inhibiting YAP-mediated oncogenic signaling pathways.

Conclusions

The present study revealed that IALT exerts its biological effects by modulating YAP activity via the canonical Hippo-LATS signaling pathway. By inducing YAP phosphorylation and subsequent cytoplasmic sequestration, IALT effectively suppresses YAP-dependent gene expression and inhibits cell growth, migration, and tumor progression. These findings provide valuable insights into the molecular mechanisms underlying the anti-tumor properties of IALT and highlight its potential as a promising therapeutic candidate for cancer treatments targeting YAP signaling. Further studies are warranted to fully elucidate the precise molecular interactions involved and explore the clinical implications of IALT in cancer therapy.

CRediT authorship contribution statement

Cho-Long Kim: Writing – review & editing, Methodology, Formal analysis, Data curation. **Su-Bin Lim:** Methodology, Formal analysis, Data curation. **Dong Hyun Kim:** Formal analysis, Data curation. **Ye Eun Sim:** Formal analysis, Data curation. **Li-Jung Kang:** Methodology, Formal analysis, Data curation. **Su Jung Park:** Writing – review & editing, Validation, Methodology. **Hyungwoo Kim:** Methodology, Formal analysis. **Tae Hoon Roh:** Writing – review & editing, Methodology, Funding acquisition. **Jung-Soon Mo:** Writing – review & editing, Supervision, Funding acquisition, Conceptualization. **Han-Sol Jeong:** Writing – original draft, Supervision, Funding acquisition, Conceptualization.

Declaration of competing interest

The authors declare no competing interests.

Acknowledgments

This work was supported by the National Research Foundation of Korea (NRF) funded by the Ministry of Science and ICT (MSIT) in Korea (NRF-2020R1A2C2011016 and 2018R1D1A1B07043856), and a Korea Basic Science Institute (National Research Facilities & Equipment Center) grant funded by the Ministry of Education (Grant Nos. 2019R1A6C1010003 and 2021R1A6C102A517). This work was supported by research fund of Ajou University Medical Center (2023).

Supplementary materials

Supplementary material associated with this article can be found, in the online version, at doi:10.1016/j.tranon.2024.101971.

References

[1] J.M. Banales, J.J.G. Marin, A. Lamarca, P.M. Rodrigues, S.A. Khan, L.R. Roberts, V. Cardinale, G. Carpino, J.B. Andersen, C. Braconi, D.F. Calvisi, M.J. Perugorria, L. Fabris, L. Boulter, R.I.R. Macias, E. Gaudio, D. Alvaro, S.A. Gradilone, M. Strazzabosco, M. Marzioni, C. Coulouarn, L. Fouassier, C. Raggi, P. Invernizzi, J. C. Mertens, A. Moncsek, S. Rizvi, J. Heimbach, B.G. Koerkamp, J. Bruix, A. Forner, J. Bridgewater, J.W. Valle, G.J. Gores, Cholangiocarcinoma 2020: the next horizon in mechanisms and management, Nat. Rev. Gastroenterol. Hepatol. 17 (2020) 557–588.

[2] K. Bum-Erdene, D. Zhou, G. Gonzalez-Gutierrez, M.K. Ghozayel, Y. Si, D. Xu, H. E. Shannon, B.J. Bailey, T.W. Corson, K.E. Pollok, C.D. Wells, S.O. Meroueh, Small-molecule covalent modification of conserved cysteine leads to allosteric inhibition of the TEAD·Yap protein-protein interaction, Cell Chem. Biol. 26 (2019) 378–389, e313.

[3] Y. Cai, K. Gao, B. Peng, Z. Xu, J. Peng, J. Li, X. Chen, S. Zeng, K. Hu, Y. Yan, Alantolactone: a natural plant extract as a potential therapeutic agent for cancer, Front. Pharmacol. 12 (2021) 781033.

[4] P. Chan, X. Han, B. Zheng, M. DeRan, J. Yu, G.K. Jarugumilli, H. Deng, D. Pan, X. Luo, X. Wu, Autopalmitoylation of TEAD proteins regulates transcriptional output of the Hippo pathway, Nat. Chem. Biol. 12 (2016) 282–289.

[5] W. Chen, P. Li, Y. Liu, Y. Yang, X. Ye, F. Zhang, H. Huang, Isoalantolactone induces apoptosis through ROS-mediated ER stress and inhibition of STAT3 in prostate cancer cells, J. Exp. Clin. Cancer Res. 37 (2018) 309.

[6] R. Cheng, Q. Du, J. Ye, B. Wang, Y. Chen, Prognostic value of site-specific metastases for patients with advanced intrahepatic cholangiocarcinoma: a SEER database analysis, Medicine 98 (2019) e18191 (Baltimore).

[7] J. Chun, Isoalantolactone suppresses glycolysis and resensitizes cisplatin-based chemotherapy in cisplatin-resistant ovarian cancer cells, Int. J. Mol. Sci. 24 (2023).

[8] C.B. Conboy, J.A. Yonkus, E.H. Buckarma, D.G. Mun, N.W. Werneburg, R. D. Watkins, R. Alva-Ruiz, J.L. Tomlinson, Y. Guo, J. Wang, D. O'Brien, C. E. McCabe, E. Jessen, R.P. Graham, R.C. Buijsman, D. Vu, J. de Man, S.I. Ilyas, M. J. Truty, M. Borad, A. Pandey, G.J. Gores, R.L. Smoot, LCK inhibition downregulates YAP activity and is therapeutic in patient-derived models of cholangiocarcinoma, J. Hepatol. 78 (2023) 142–152.

[9] R. Cunningham, C.G. Hansen, The Hippo pathway in cancer: YAP/TAZ and TEAD as therapeutic targets in cancer, Clin. Sci. 136 (2022) 197–222 (Lond.).

[10] Y.H. Ding, Y.D. Song, Y.X. Wu, H.Q. He, T.H. Yu, Y.D. Hu, D.P. Zhang, H.C. Jiang, K.K. Yu, X.Z. Li, L. Sun, F. Qian, Isoalantolactone suppresses LPS-induced inflammation by inhibiting TRAF6 ubiquitination and alleviates acute lung injury, Acta Pharmacol. Sin. 40 (2019) 64–74.

[11] S. Dutta, S. Mahalanobish, S. Saha, S. Ghosh, P.C. Sil, Natural products: an upcoming therapeutic approach to cancer, Food Chem. Toxicol. 128 (2019) 240–255.
[12] J.M. Franklin, Z. Wu, K.L. Guan, Insights into recent findings and clinical application of YAP and TAZ in cancer, Nat. Rev. Cancer 23 (2023) 512–525.
[13] T.J. Hagenbeek, J.R. Zbieg, M. Hafner, R. Mroue, J.A. Lacap, N.M. Sodir, C. L. Noland, S. Afghani, A. Kishore, K.P. Bhat, X. Yao, S. Schmidt, S. Clausen, M. Steffek, W. Lee, P. Beroza, S. Martin, E. Lin, R. Fong, P. Di Lello, M.H. Kubala, M.N. Yang, J.T. Lau, E. Chan, A. Arrazate, L. An, E. Levy, M.N. Lorenzo, H.J. Lee, T. H. Pham, Z. Modrusan, R. Zang, Y.C. Chen, M. Kabza, M. Ahmed, J. Li, M.T. Chang, D. Maddalo, M. Evangelista, X. Ye, J.J. Crawford, A. Dey, An allosteric pan-TEAD inhibitor blocks oncogenic YAP/TAZ signaling and overcomes KRAS G12C inhibitor resistance, Nat. Cancer 4 (2023) 812–828.
[14] L. Jiang, J. Zhang, Q. Xu, B. Wang, Y. Yao, L. Sun, X. Wang, D. Zhou, L. Gao, S. Song, X. Zhu, YAP promotes the proliferation and migration of colorectal cancer cells through the Glut3/AMPK signaling pathway, Oncol. Lett. 21 (2021) 312.
[15] W. Ketai, L. Huitao, Z. Yunkun, C. Xingguo, H. Zhide, S. Yucheng, M. Xiao, Separation and determination of alantolactone and isoalantolactone in traditional Chinese herbs by capillary electrophoresis, Talanta 52 (2000) 1001–1005.
[16] M. Khan, C. Ding, A. Rasul, F. Yi, T. Li, H. Gao, R. Gao, L. Zhong, K. Zhang, X. Fang, T. Ma, Isoalantolactone induces reactive oxygen species mediated apoptosis in pancreatic carcinoma PANC-1 cells, Int. J. Biol. Sci. 8 (2012) 533–547.
[17] C.L. Kim, S.H. Choi, J.S. Mo, Role of the Hippo pathway in fibrosis and cancer, Cells 8 (2019).
[18] C.L. Kim, Y.S. Shin, S.H. Choi, S. Oh, K. Kim, H.S. Jeong, J.S. Mo, Extracts of Perilla frutescens var. Acuta (Odash.) kudo leaves have antitumor effects on breast cancer cells by suppressing YAP activity, Evid. Based Complement. Alternat. Med. 2021 (2021) 5619761.
[19] M.Y. Kim, H. Lee, S.Y. Ji, S.Y. Kim, H. Hwangbo, S.H. Park, G.Y. Kim, C. Park, S. H. Leem, S.H. Hong, Y.H. Choi, Induction of apoptosis by isoalantolactone in human hepatocellular carcinoma Hep3B cells through activation of the ROS-dependent JNK signaling pathway, Pharmaceutics 13 (2021).
[20] F. Koinis, E. Chantzara, M. Samarinas, A. Xagara, Z. Kratiras, V. Leontopoulou, A. Kotsakis, Emerging role of YAP and the Hippo pathway in prostate cancer, Biomedicines 10 (2022).
[21] J. Li, P. Zhu, Y. Chen, S. Zhang, Z. Zhang, Z. Zhang, Y. Wang, X. Jiang, K. Lin, W. Wu, Z. Mo, S.C.W. Sze, K.K.L. Yung, Isoalantolactone induces cell cycle arrest, apoptosis and autophagy in colorectal cancer cells, Front. Pharmacol. 13 (2022) 903599.
[22] Z. Li, B. Qin, X. Qi, J. Mao, D. Wu, Isoalantolactone induces apoptosis in human breast cancer cells via ROS-mediated mitochondrial pathway and downregulation of SIRT1, Arch. Pharm. Res. 39 (2016) 1441–1453.
[23] C.H. Liu, A.K. Mishra, R.X. Tan, C. Tang, H. Yang, Y.F. Shen, Repellent and insecticidal activities of essential oils from Artemisia princeps and Cinnamomum camphora and their effect on seed germination of wheat and broad bean, Bioresour. Technol. 97 (2006) 1969–1973.
[24] Y. Liu, B. Zhang, Y. Zhou, Y. Xing, Y. Wang, Y. Jia, D. Liu, Targeting Hippo pathway: a novel strategy for Helicobacter pylori-induced gastric cancer treatment, Biomed. PharmacOther 161 (2023) 114549.
[25] P. Marti, C. Stein, T. Blumer, Y. Abraham, M.T. Dill, M. Pikiolek, V. Orsini, G. Jurisic, P. Megel, Z. Makowska, C. Agarinis, L. Tornillo, T. Bouwmeester, H. Ruffner, A. Bauer, C.N. Parker, T. Schmelzle, L.M. Terracciano, M.H. Heim, J. S. Tchorz, YAP promotes proliferation, chemoresistance, and angiogenesis in human cholangiocarcinoma through TEAD transcription factors, Hepatology 62 (2015) 1497–1510.
[26] N.A. McGrath, J. Fu, S.Z. Gu, C. Xie, Targeting cancer stem cells in cholangiocarcinoma (Review), Int. J. Oncol. 57 (2020) 397–408.
[27] X. Miao, C. Liu, Y. Jiang, Y. Wang, D. Kong, Z. Wu, X. Wang, R. Tian, X. Yu, X. Zhu, W. Gong, BET protein inhibition evidently enhances sensitivity to PI3K/mTOR dual inhibition in intrahepatic cholangiocarcinoma, Cell Death Dis. 12 (2021) 1020.
[28] J.S. Mo, Z. Meng, Y.C. Kim, H.W. Park, C.G. Hansen, S. Kim, D.S. Lim, K.L. Guan, Cellular energy stress induces AMPK-mediated regulation of YAP and the Hippo pathway, Nat. Cell Biol. 17 (2015) 500–510.
[29] S. Mouillet-Richard, P. Laurent-Puig, YAP/TAZ signalling in colorectal cancer: lessons from consensus molecular subtypes, Cancers (2020) 12 (Basel).
[30] A.T. Nguyen-Lefebvre, N. Selzner, J.L. Wrana, M. Bhat, The hippo pathway: a master regulator of liver metabolism, regeneration, and disease, FASEB J. 35 (2021) e21570.
[31] S.W. Plouffe, Z. Meng, K.C. Lin, B. Lin, A.W. Hong, J.V. Chun, K.L. Guan, Characterization of Hippo pathway components by gene inactivation, Mol. Cell 64 (2016) 993–1008.
[32] A.V. Pobbati, R. Kumar, B.P. Rubin, W. Hong, Therapeutic targeting of TEAD transcription factors in cancer, Trends. Biochem. Sci. 48 (2023) 450–462.
[33] A. Rasul, M. Khan, M. Ali, J. Li, X. Li, Targeting apoptosis pathways in cancer with alantolactone and isoalantolactone, Sci. World J. 2013 (2013) 248532.
[34] A. Rasul, M. Khan, B. Yu, M. Ali, Y.J. Bo, H. Yang, T. Ma, Isoalantolactone, a sesquiterpene lactone, induces apoptosis in SGC-7901 cells via mitochondrial and phosphatidylinositol 3-kinase/Akt signaling pathways, Arch. Pharm. Res. 36 (2013) 1262–1269.
[35] S. Rizvi, D. Yamada, P. Hirsova, S.F. Bronk, N.W. Werneburg, A. Krishnan, W. Salim, L. Zhang, E. Trushina, M.J. Truty, G.J. Gores, A Hippo and fibroblast growth factor receptor autocrine pathway in cholangiocarcinoma, J. Biol. Chem. 291 (2016) 8031–8047.
[36] S. Saikawa, K. Kaji, N. Nishimura, K. Seki, S. Sato, K. Nakanishi, K. Kitagawa, H. Kawaratani, M. Kitade, K. Moriya, T. Namisaki, A. Mitoro, H. Yoshiji, Angiotensin receptor blockade attenuates cholangiocarcinoma cell growth by inhibiting the oncogenic activity of Yes-associated protein, Cancer Lett. 434 (2018) 120–129.
[37] R.L. Siegel, K.D. Miller, N.S. Wagle, A. Jemal, Cancer statistics, 2023, CA Cancer J. Clin. 73 (2023) 17–48.
[38] R.L. Smoot, N.W. Werneburg, T. Sugihara, M.C. Hernandez, L. Yang, C. Mehner, R. P. Graham, S.F. Bronk, M.J. Truty, G.J. Gores, Platelet-derived growth factor regulates YAP transcriptional activity via Src family kinase dependent tyrosine phosphorylation, J. Cell Biochem. 119 (2018) 824–836.
[39] T. Sugihara, H. Isomoto, G. Gores, R. Smoot, YAP and the Hippo pathway in cholangiocarcinoma, J. Gastroenterol. 54 (2019) 485–491.
[40] K. Sugiura, T. Mishima, S. Takano, H. Yoshitomi, K. Furukawa, T. Takayashiki, S. Kuboki, M. Takada, M. Miyazaki, M. Ohtsuka, The expression of yes-associated protein (YAP) maintains putative cancer stemness and is associated with poor prognosis in intrahepatic cholangiocarcinoma, Am. J. Pathol. 189 (2019) 1863–1877.
[41] Y. Sun, L. Hu, Z. Tao, G.K. Jarugumilli, H. Erb, A. Singh, Q. Li, J.L. Cotton, P. Greninger, R.K. Egan, Y. Tony Ip, C.H. Benes, J. Che, J. Mao, X. Wu, Pharmacological blockade of TEAD-YAP reveals its therapeutic limitation in cancer cells, Nat. Commun. 13 (2022) 6744.
[42] N.U. Tariq, M.G. McNamara, J.W. Valle, Biliary tract cancers: current knowledge, clinical candidates and future challenges, Cancer Manage Res. 11 (2019) 2623–2642.
[43] M. Toth, L. Wehling, L. Thiess, F. Rose, J. Schmitt, S.M.E. Weiler, C. Sticht, C. De La Torre, M. Rausch, T. Albrecht, N. Grabe, L. Duwe, J.B. Andersen, B.C. Kohler, C. Springfeld, A. Mehrabi, Y. Kulu, P. Schirmacher, S. Roessler, B. Goeppert, K. Breuhahn, Co-expression of YAP and TAZ associates with chromosomal instability in human cholangiocarcinoma, BMC Cancer 21 (2021) 1079.
[44] J.W. Valle, R.K. Kelley, B. Nervi, D.Y. Oh, A.X. Zhu, Biliary tract cancer, Lancet 397 (2021) 428–444.
[45] A. Vogel, A. Saborowski, Current and future systemic therapies in biliary tract cancer, Visc. Med. 37 (2021) 32–38.
[46] T. Wang, C. Xu, Z. Zhang, H. Wu, X. Li, Y. Zhang, N. Deng, N. Dang, G. Tang, X. Yang, B. Shi, Z. Li, L. Li, K. Ye, Cellular heterogeneity and transcriptomic profiles during intrahepatic cholangiocarcinoma initiation and progression, Hepatology 76 (2022) 1302–1317.
[47] Z. Weng, H. Gao, J. Hu, Y. Fan, H. Wang, L. Li, Isoalantolactone induces autophagic cell death in SKOV(3) human ovarian carcinoma cells via upregulation of PEA-15, Oncol. Rep. 35 (2016) 833–840.
[48] H. Wu, Y. Liu, Z. Liao, J. Mo, Q. Zhang, B. Zhang, L. Zhang, The role of YAP1 in liver cancer stem cells: proven and potential mechanisms, Biomark. Res. 10 (2022) 42.
[49] M. Wu, H. Zhang, J. Hu, Z. Weng, C. Li, H. Li, Y. Zhao, X. Mei, F. Ren, L. Li, Isoalantolactone inhibits UM-SCC-10A cell growth via cell cycle arrest and apoptosis induction, PLoS One 8 (2013) e76000.
[50] Z.C. Wu, X.G. Hui, L. Huo, D.X. Sun, W. Peng, Y. Zhang, X.B. Li, T. Ma, W.H. Li, J. Liang, Z.Q. Sun, Antiproliferative effects of isoalantolactone in human liver cancer cells are mediated through caspase-dependent apoptosis, ROS generation, suppression of cell migration and invasion and targeting Ras/Raf/MEK signalling pathway, Acta Biochim. Pol. 69 (2022) 299–304.
[51] C.B. Yuan, L. Tian, B. Yang, H.Y. Zhou, Isoalantolactone protects LPS-induced acute lung injury through Nrf2 activation, Microb. Pathog. 123 (2018) 213–218.
[52] C. Zhang, L. Huang, J. Xiong, L. Xie, S. Ying, Y. Jia, Y. Yao, X. Song, Z. Zeng, J. Yuan, Isoalantolactone inhibits pancreatic cancer proliferation by regulation of PI3K and Wnt signal pathway, PLoS One 16 (2021) e0247752.
[53] S. Zhang, X. Song, D. Cao, Z. Xu, B. Fan, L. Che, J. Hu, B. Chen, M. Dong, M.G. Pilo, A. Cigliano, K. Evert, S. Ribback, F. Dombrowski, R.M. Pascale, A. Cossu, G. Vidili, A. Porcu, M.M. Simile, G.M. Pes, G. Giannelli, J. Gordan, L. Wei, M. Evert, W. Cong, D.F. Calvisi, X. Chen, Pan-mTOR inhibitor MLN0128 is effective against intrahepatic cholangiocarcinoma in mice, J. Hepatol. 67 (2017) 1194–1203.